ADVANCES IN ATMOSPHERIC SCIENCES, VOL. 21, NO. 6, 2004, 951–963

The Structure and Rainfall Features of Tropical Cyclone Rammasun (2002)

MA Leiming* (马雷鸣), DUAN Yihong (端义宏), and ZHU Yongti (朱永禔)

Shanghai Typhoon Institute, Shanghai 200030

(Received 6 November 2003; revised 8 March 2004)

ABSTRACT

Tropical Rainfall Measuring Mission (TRMM) data [TRMM Microwave Imager/Precipitation Radar/Visible and Infrared Scanner (TMI/PR/VIRS)] and a numerical model are used to investigate the structure and rainfall features of Tropical Cyclone (TC) Rammasun (2002). Based on the analysis of TRMM data, which are diagnosed together with NCEP/AVN [Aviation (global model)] analysis data, some typical features of TC structure and rainfall are preliminary discovered. Since the limitations of TRMM data are considered for their time resolution and coverage, the world observed by TRMM at several moments cannot be taken as the representation of the whole period of the TC lifecycle, therefore the picture should be reproduced by a numerical model of high quality. To better understand the structure and rainfall features of TC Rammasun, a numerical simulation is carried out with mesoscale model MM5 in which the validations have been made with the data of TRMM and NCEP/AVN analysis.

Key words: TC Rammasun, TRMM, rainfall, Cumulus parameterization scheme, numerical simulation, precipitable water

1. Introduction

Rainfall measurement over the Tropics is important for tropical weather and climate studies. However, accurate measurement of the spatial and temporal variations of tropical rainfall has been a critical problem in tropical meteorology until the launch of the Tropical Rainfall Measuring Mission (TRMM) in 1997. During TRMM's expected six-year mission, its broad sampling footprint between 35°N and 35°S has been providing the first detailed and comprehensive dataset on the four-dimensional distribution of rainfall and latent heating over the vastly unsampled tropical oceanic and continental regions. TRMM offers a unique opportunity to improve the understanding of tropical meteorology and to evaluate the impact of rainfall data on tropical weather forecasts. In recent years, TRMM data have been applied in tropical cyclone research (Rogers et al., 2000; Marécal and Mahfouf, 2001) and in simulation of heavy rainfall (Xu et al., 2003). TRMM/PR images were also used (Jin et al., 2003) to analyze the structure and synoptic characteristic of a frontal rain belt during 1998 GEWEX Asian Monsoon Experiment/Huaihe river Basin EXperiment (GAME/HUBEX). It is inspiring that the TRMM/TRMM Microwave Imager (TMI) rainfall rate has been used to improve the simulation of tropical cyclones in terms of their intensity and kinematical and precipitation structures (Pu et al., 2002). Although continuous progress has been made, the knowledge of Tropical Cyclone (TC) structure and rainfall is still limited. Few people have investigated the four-dimensional rainfall features and structures of tropical cyclones with TRMM data.

The structure and rainfall features of TC Rammasun are studied in this paper, which is organized as follows. Section 2 briefly introduces the TRMM data. Section 3 outlines on the background and evolution processes of TC Rammasun using TRMM images and NCEP/AVN [Aviation (global model)] analysis. Section 4 investigates the 3-D structure of rainfall and precipitable water by TRMM. Section 5 diagnoses the relationship between rainfall and Slantwise Convective Available Potential Energy (SCAPE) with TRMM and NCEP/AVN data. Section 6 validates the MM5 model. Section 7 gives a preliminary analysis on the structure and rainfall features of TC Rammasun. Section 8 draws some conclusions.

2. TRMM data

TRMM is a joint project by the National Aero-

*E-mail: malm@mail.typhoon.gov.cn

nautics and Space Administration (NASA, U.S.A) and the National Space Development Agency of Japan (NASDA). The main objective of this mission is to improve the measurement of tropical precipitation and energy exchange (Simpson et al., 1996). The TRMM satellite launched on 27 November 1997 has a near circular orbit with altitude 350 km ranging between 35°N and 35°S of the equator.

Aboard TRMM are five instruments among which PR (Precipitation Radar), TMI, and VIRS (Visible and Infrared System) are the three primary instruments that constitute a rainfall measurement package (Kummerow et al., 1998).

TRMM/PR has a horizontal resolution at the ground of about 4 km and a swath width of 220 km. One of its most important features is its ability to provide vertical profiles of the rain from the surface up to a height of about 20 km. TRMM/TMI can make quantitative measurement of surface rainfall rate and 3-D precipitable water (PW) with a swath width of 760 km. TRMM/VIRS, with a swath width of 720 km, can provide cloud distributions at a horizontal resolution of 2.1 km (nadir).

Surface rainfall rate and 3-D PW data by TRMM/TMI (at 0000 UTC 28 June, 0000 UTC 2 July, 0000 UTC 3 July, 1500 UTC 3 July, 1500 UTC 4 July 2002), 3-D rainfall rate data by TRMM/PR (at 1500 UTC 3 July 2002) and cloud images by TRMM/VIRS (at 0000 UTC 28 June, 1500 UTC 4 July 2002) are used in this study.

3. TC Rammasun

To better understand the background of TC Rammasun's development, TRMM data and NCEP/AVN analysis are given a brief overview in this section.

TC Rammasun was activated simultaneously with TC Matmo farther east in the vicinity of Chuuk. The developments of both systems were related to a strong surge in the monsoonal westerlies. At 0000 UTC 26 June, a low-level convective center (LLCC) was located in the east-northeast of Palau and embedded in a convergence line caused by the enhanced equatorial westerlies and tropical easterlies. At 0000 UTC 28 June 2002, Rammasun developed as a tropical depression at about 250 km northwest of Yap and developed into a tropical storm on 0000 UTC 29 June 2002 (Fig. 1).

The storm moved northwestwards over the Pacific and strengthened gradually into a typhoon at 1200 UTC 1 July. Rammasun moved steadily northwestward

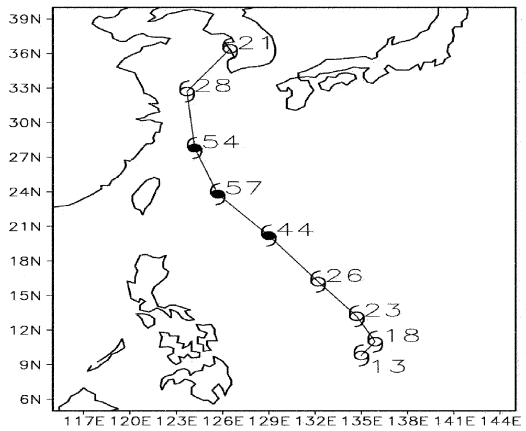

Fig. 1. The best track of TC Rammasun, which starts with 0000 UTC 28 June 2002 at a 24-h interval. The number beside each TC mark denotes the maximum wind speed (units: m s^{-1}) near the TC center.

at around 22–26 km h^{-1} throughout the period of 2 July, gradually intensifying. During this period, TRMM/VIRS revealed that the storm had developed an eye. Rammasun reached its peak intensity of 57 m s^{-1} when it was centered approximately 509 km east-southeast of Taiwan. The torrential rain associated with Rammasun caused flooding and landslides in northern Taiwan. The storm remained at peak intensity for 30 hours and continued to move northwestward at a slower pace, steered by an eastern subtropical ridge, with plenty of water vapor transported by two air flows from the southwest and northeast (Fig. 2a). The wind field around the TC center was asymmetrical, being stronger in the north and weaker in the south (Fig. 2b). Influenced by a quasi-stationary long wave trough over the Chinese coast (Fig. 2a), Rammasun turned toward the north-northwest, weakening in the ridge of a subtropical high. By 0000 UTC on 4 July, Rammasun was located a little more than 350 km northwest of Okinawa, moving north-northwestward at 20 km h^{-1}. The western semicircle of the storm was influenced more obviously by the longwave trough. Then Rammasun turned north and moved across the East China Sea. At 1500 UTC 4 July, the TRMM/VIRS image indicates that the eye had disappeared. At 0000 UTC 5 July, Rammasun weakened into a tropical storm and accelerated north-northeastward. By 6 July, in response to a major shortwave trough, Rammasun moved toward the Russian coast and made landfall over the west coast of South Korea.

4. The 3-D structure of precipitable water and rainfall by TRMM

The PW structure of TC Rammasun is shown in

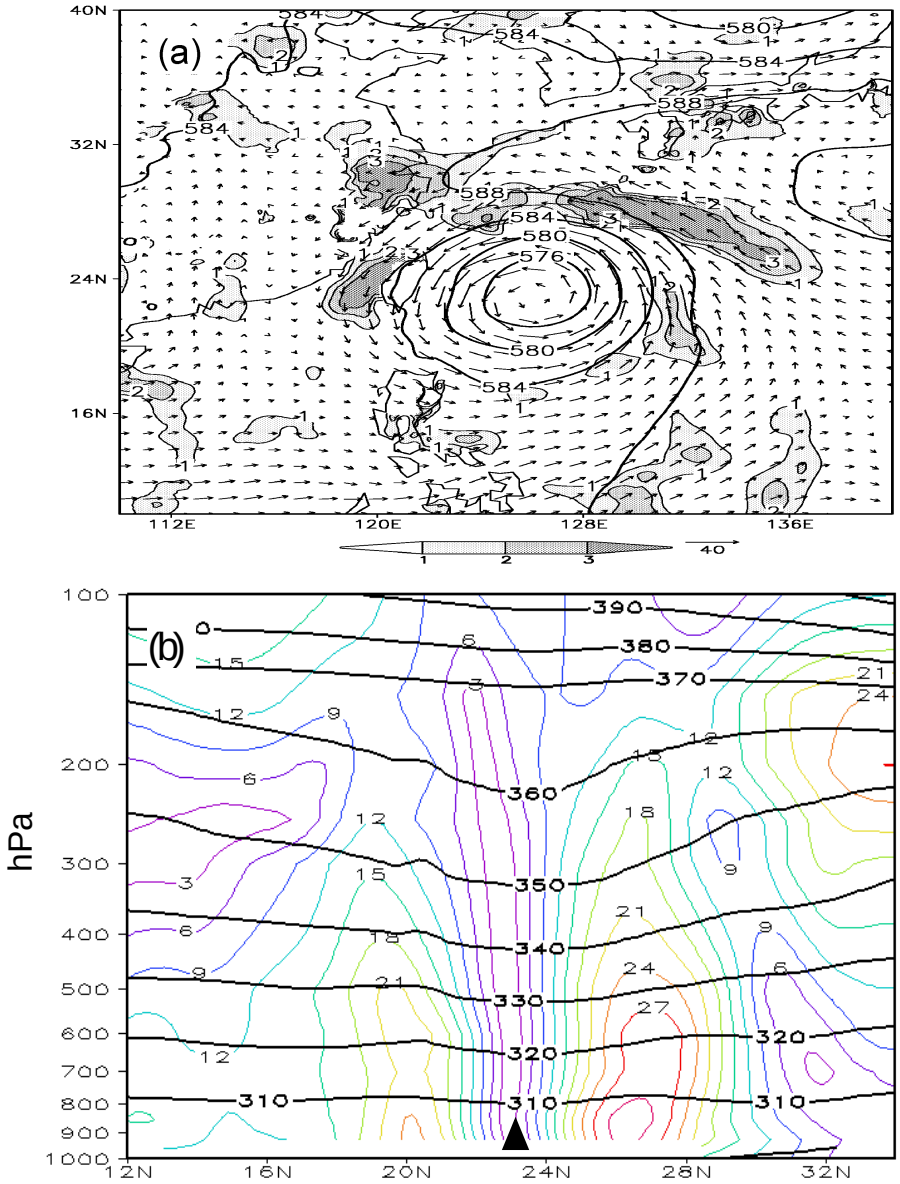

Fig. 2. (a) 500-hPa heights (units: 10 gpm) and 925 hPa–700 hPa averaged divergence of water vapor flux (units: 10^{-7} g cm^{-2} hPa^{-1} s^{-1}), (b) meridional vertical cross section of potential temperature (units: K, thick line) and horizontal wind speed (units: m s^{-1}, slim line) through the center of the TC (solid triangle) at 0000 UTC 3 July 2002.

Fig. 3. At 0000 UTC 28 June (Fig. 3a, the time of the formation of the tropical depression), there are two organized parts of PW near the tropical low. The south one is distributed as a long belt and the north one looks like a comma mark, the characteristic of which is similar to the distribution of surface rainfall rate shown in Fig. 5a. There is much PW (1000 mg m^{-3}) in the west of the south belt and little PW in the east (750 mg m^{-3}), which indicates that a possible LLCC is embedded in a line of convergent flow caused by the enhanced equatorial westerlies and tropical easterlies. By the time the tropical storm has been formed, these two belts of PW have joined together. An asymmetric feature is indicated by the distribution of PW, the maximum value of which around the TC center (1250 mg m^{-3}) is higher in the east quadrant than in the west (1000 mg m^{-3}), which indicates a stronger convection in the east. Despite this, the depression system

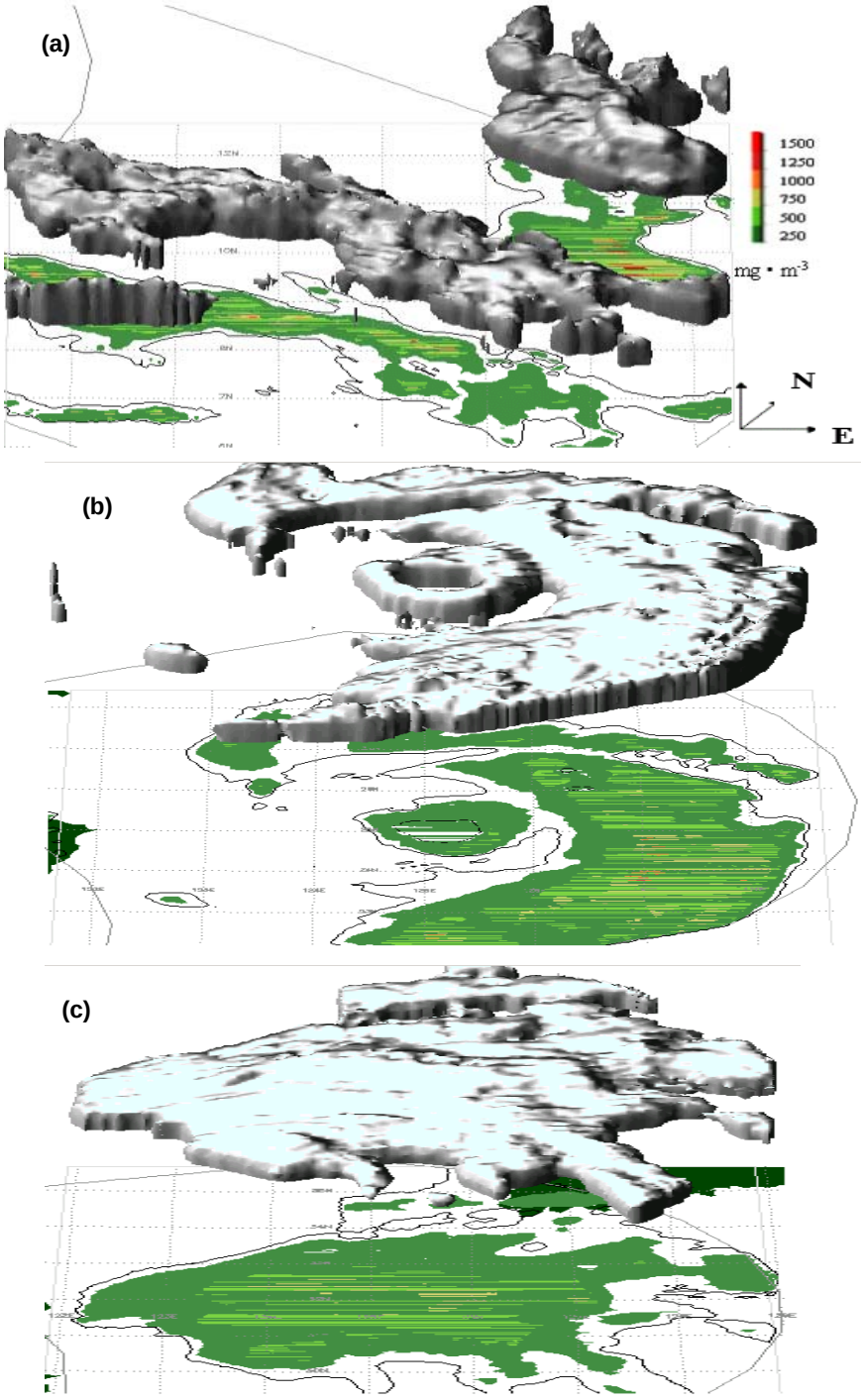

Fig. 3. Three-dimensional precipitable water (units: mg m^{-3}) derived by TRMM/TMI at (a) 0000 UTC 28 June, (b) 1500 UTC 3 July and (c) 1500 UTC 4 July 2002.

became united and came to a period of steady development. At 1500 UTC 3 July 2002, TC Rammasun reached the status of being a typhoon with an eyewall (Fig. 3b), around which the PW value is high. The asymmetric feature of the TC center is more evident with the high PW value in the east, the maximum of which is located about 1.5–2.5° of longitude toward the center. There is a blank zone of PW between the eyewall and eastern high, the distribution of which is similar to that of the rainfall bands by TMI (Fig. 4c). The high value of PW is exactly located in the area of intensive rainfall, while heavy rainfall only occurs in the area of organized PW bands. At 1500 UTC 4 July 2002, Rammasun degraded into a tropical storm with the uniform distribution of PW (average value of 750 mg m^{-3}), where no heavy rainfall existed (Fig. 3c).

Because of the limitation of TRMM/PR's coverage and time resolution for some limited area covered by TC, only one picture covers the center of the TC during its mature period (Figs. 4a–b). Figure 4b shows that the highest intensity of rainfall rate is concentrated under 7.5 km above the sea surface, where the distribution of the rainfall rate is uniform. About 1–2° of longitude to the east of the eye, a broad periphery

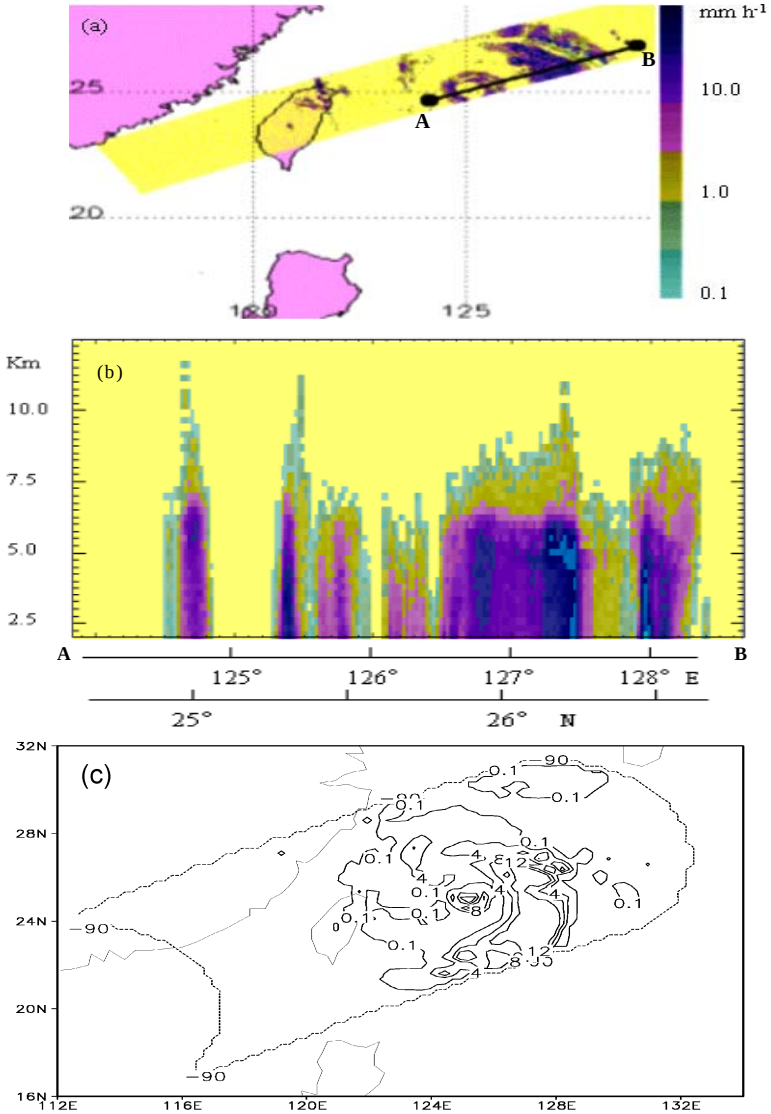

Fig. 4. (a) Surface rainfall rate (units: mm h^{-1}) by TRMM/PR, and the position of the cross section (the thick line connecting A and B) across the TC center; (b) Rainfall rate along the cross section shown in (a), the color bar is the same as in (a); (c) Surface rainfall rate by TRMM/TMI (dotted line indicates TRMM/PR's coverage.) All three figures are for 1500 UTC 3 July 2002.

rainfall belt exists, the surface value of which (14 mm h^{-1}) is higher than that near the eyewall (8 mm h^{-1}) (Fig. 4c). The eastern periphery rain belt has an evident high value center (10–20 mm h^{-1})near the 5 km height above the sea surface. Particularly, rainfall around the eye extends to a higher level (above 10 km) than the eastern periphery rainfall belt (under 10 km).

5. Rainfall and SCAPE

Energy should be provided during the intensification of a TC, and this is related closely with rainfall. Assumed to be an index of this energy, SCAPE (Emanuel, 1983b) is diagnosed and joined with TRMM/TMI surface rainfall.

Convective Available Potential Energy (CAPE) provides a measure of the maximum possible kinetic energy that a parcel can acquire(Emanuel,1983a), starting from rest and moving vertically due to gravitational convection. SCAPE is the slantwise convection analogue of CAPE. It is calculated assuming that the parcel moves up through the environment following a slantwise path along an absolute angular momentum surface. In the case of CAPE, the parcel is assumed to rise vertically. The maximum energy that a parcel can obtain as it rises corresponds to the positive area in the tephigram, which is surrounded by the moist adiabat line and the sounding temperature curve in the middle of the level of free convection (LFC) and the level of neutral buoyancy (LNB).

SCAPE is supposed to fit for TC's slantwise environment, and should be taken as an indicator of the susceptibility to slantwise convection rather than the actual kinetic energy that the parcel would attain. SCAPE can also be calculated from numerical weather prediction (NWP) model fields (Shutts, 1990).

$$E_{\mathrm{SCAPE}} = \frac{g}{\theta_{\mathrm{v,env}}} \int_{\mathrm{LFC}}^{\mathrm{LNB}} (\theta_{\mathrm{v,parcel}} - \theta_{\mathrm{v,env}}) dz \ , \quad (1)$$

$\theta_{\mathrm{v,env}}$ is potential temperature of the environment; $\theta_{\mathrm{v,parcel}}$ is potential temperature of the air parcel.

NCEP/AVN analysis data are then used in Eq. (1) to calculate the SCAPE of TC Rammasun, which is diagnosed with rainfall by TRMM/TMI at the same time (0000 UTC 28 June 2002, 0000 UTC 2 July 2002, 0000 UTC 3 July 2002) (Fig. 5).

At 0000 UTC 28 June 2002, two major rain belts are located in the area of the tropical depression (Fig. 5a) which has been analyzed in Section 4. The maximum rainfall rate (8 mm h^{-1}) of the south belt is at (9.9°N, 130.1°E), which is identically in the area of the high value of SCAPE (1200 J kg^{-1}). The maximum rainfall rate (8 mm h^{-1}) of the north belt is at (10.2°N, 135.9°E). At 0000 UTC 2 July 2002 (Fig. 5b), the

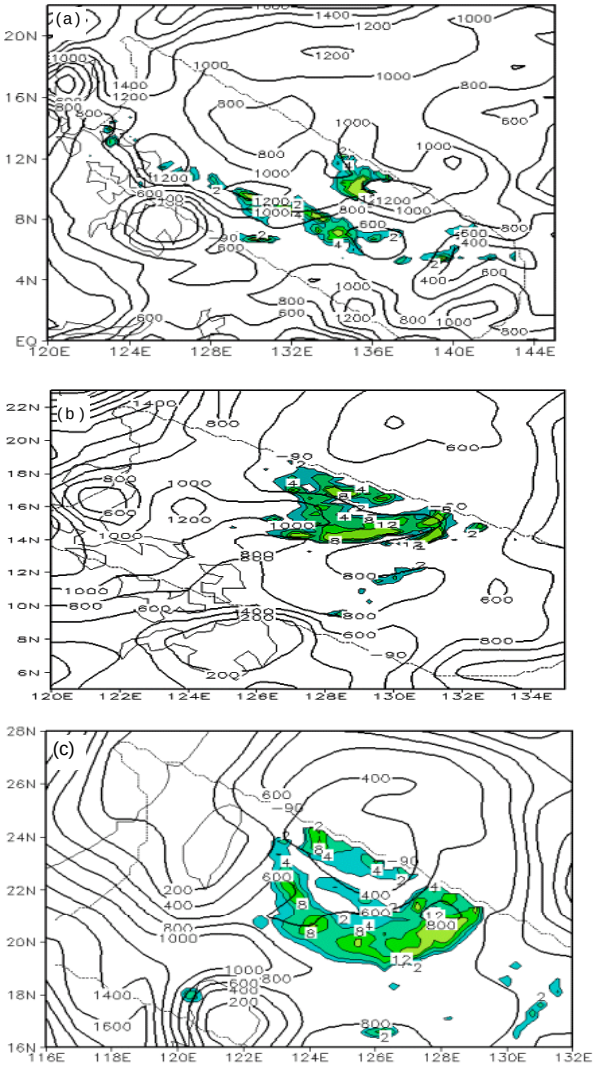

Fig. 5. Surface rainfall rate by TRMM/TMI (mm h^{-1}, shaded) and SCAPE values (J kg^{-1}, isolines) by NCEP/AVN at (a) 0000 UTC 28 June, (b) 0000 UTC 2 July and (c) 00:00 UTC 3 July 2002.

maximum rainfall rate (12 mm h^{-1}) is at (14.2°N, 129.7°E), which is identical with the area of the "tongue" of high SCAPE (800 J kg^{-1}). At 0000 UTC 3 July 2002 (Fig. 5c), the maximum value of rainfall rate (12 mm h^{-1}) is also located in the position of highest SCAPE (800 J kg^{-1}).

It can be seen from the above analysis that the high positive SCAPE is located identically in the area of high rainfall rate.

6. Model validation by TRMM and NCEP data

Successful simulation of precipitation is one of the most important criterions to evaluate the capability of mesoscale models to depict TC structure. This simulation can be improved by choosing better parameter-

ization schemes (Weygandt and Seaman, 1994), which can greatly impact the rainfall prediction (Kuo, 1996).

Because of the lack of precipitation data observed in the sea area before the launch of TRMM, few people have investigated the capability of numerical models in TC Quantitative Precipitation Forecasting (QPF). In this section, several numerical experiments are carried out with Pennsylvania State University (PSU)/NCAR MM5 (Grell, 1994), on which the validation is performed especially for its cumulus parameterization schemes.

6.1 *Experiment design*

A single mesh domain with 27-km grid spacing (151×151 grid points) is employed to achieve the simulation. The domain center is located at (25°N, 125°E). The vertical structure of the model comprises 23 σ levels with the top of the model set at a pressure of 10 hPa. The σ levels are placed at values of 1.0, 0.99, 0.97, 0.94, 0.92, 0.90, 0.88, 0.86, 0.81, 0.75, 0.69, 0.63, 0.57, 0.51, 0.45, 0.39, 0.33, 0.27, 0.21, 0.15, 0.10, 0.06, 0.03. The main options of the physics used for this study include the MRF planetary boundary layer parameterization scheme and the cloud atmospheric radiation scheme (Dudhia, 1993).

Four experiments are carried out without (Expt. NC) and with the cumulus parameterization schemes, among which three experiments (Table 1) including the cumulus parameterization schemes considered to be fit for horizontal resolutions higher than 30 km. These three experiments are listed as Expt. GR (Grell, 1993), Expt. FC (Fritsch and Chappell, 1980) and Expt. KF (Kain and Fritsch,1993).

The initial meteorological conditions and background fields of the model are provided by NCEP/AVN analysis (horizontal resolution of 1°×1°), which can be taken as the real state of the atmosphere and another complementary resource for model validation. As an obvious vortex is contained in the field of NCEP/AVN analysis (Fig. 2), and since man-made distortion should be avoided, no bogus TC is included in the initial field.

The simulation concentrates on the period between 0000 UTC 3 July 2002 and 0000 UTC 5 July 2002, during which TC Rammasun remained at its peak intensity of 57 m s^{-1} (the maximum wind speed near the TC center) for 30 hours and made an abrupt turn toward the north-northwest. At 1500 UTC 3 July 2002, TC Rammasun happened to be covered by TRMM, and so the 3-D rainfall data can be used to validate the MM5 model.

6.2 *Validation of prediction of rainfall with TRMM data*

The surface rainfall rate at 1500 UTC 3 July 2002 is simulated in four numerical experiments, which are compared with rainfall data by TRMM in Fig. 6. The figure shows that the intensity and main area of rainfall are simulated successfully except for the absence of rainfall around the eye.

For the comparison, the PMR (position of maximum rainfall rate) and VMR (value of maximum rainfall rate) are shown in Table 2, in which the rainfall area of the TC is divided into four equal quadrants: northeast quadrant (Q1), northwest quadrant (Q2), southwest quadrant (Q3) and southeast quadrant (Q4).

For PMR, Expt. KF makes the best simulation in quadrants Q1 and Q3. The feature of heavy rainfall 1.5–2.5° of longitude to the east side of the eye is also reproduced in Expt. KF. On the contrary, Expt. NC makes the worst simulation, making quadrant Q2 a heavy rain area, where few rain is observed by TRMM. Expt. GR performs the best in quadrant Q4, while Expt. FC performs the best in quadrant Q1.

Table 1. The characteristics of cumulus parameterization schemes for the three experiments.

Exp.	Characteristics
GR	Based on rate of destabilization or quasi-equilibrium, simple single-cloud scheme with updraft and downdraft fluxes and compensating motion determine eating/moistening profile. Useful for smaller grid sizes 10-30 km, tends to allow a balance between resolved scale rainfall and convective rainfall. Shear effects on precipitation efficiency are considered. (Grell, 1993)
FC	Based on relaxation to a profile due to updraft, downdraft and subsidence region properties. The convective mass flux removes 50% of available buoyant energy in the relaxation time. Fixed entrainment rate. Suitable for 20–30 km scales due to single-cloud assumption and local subsidence. This scheme predicts both updraft and downdraft properties and also detrains cloud and precipitation. Shear effects on precipitation efficiency are also considered. (Fritsch and Chappell,1980)
KF	The KF scheme parameterizes deep convection by mixing the environmental air with convective updrafts and downdrafts to compute the net effect of convection on the model variables. (Kain and Fritsch, 1993)

Table 2. TPMR and VMR by TRMM/TMI and numerical experiments.

		TRMM/TMI	Expt. NC	Expt. GR	Expt. FC	Expt. KF
PMR	Q1	26.1°N, 126.7°E	26.5°N, 126.3°E	27.5°N, 125.4°E	26.4°N, 125.9°E	25.8°N, 126.5°E
	Q2	27.5°N, 123.4°E	28.0°N, 123.8°E	24.1°N, 124.6°E	26.3°N, 124.8°E	26.2°N, 124.0°E
	Q3	22.1°N, 124.9°E	22.7°N, 124.5°E	22.4°N, 124.5°E	22.3°N, 124.8°E	22.1°N, 124.8°E
	Q4	23.2°N, 127.1°E	22.4°N, 125.3°E	23.2°N, 127.0°E	24.1°N, 127.0°E	23.0°N, 126.9°E
VMR	Q1	14.3	14.8	13.6	13.7	14.1
(mm h^{-1})	Q2	5.2	14.7	14.5	12.1	8.3
	Q3	12.5	14.2	14.3	8.5	7.5
	Q4	14.8	14.3	14.4	12.3	14.4

As for the VMR, Expt. KF does the best in quadrants Q1 and Q4, while Expt. NC does the worst, producing heavy rainfall in all quadrants. The characteristic of the minor rainfall in quadrants Q2 and Q3 is clearly represented in Expt. KF.

Successful prediction is also done at 1500 UTC 4 July 2002 by Expt. KF for the surface rainfall rate, whose maximum value (13.9 mm h^{-1}) is located at (31.9°N, 125.6°E) near to the maximum value (14.5 mm h^{-1}) and position (32.1°N, 125.8°E) of TRMM/TMI rainfall.

The results of the above experiments may support, to a certain extent, the assumption presented by Kuo et al. (1996) and Wang and Seaman (1997) that the KF scheme depicts the complicated environment very well in which convection activity is involved (which contributes to the genesis of rainfall).

6.3 *Validation of TC structure with NCEP/AVN analysis*

From the above experiments, we can see that the model with the Kain-Fritsch cumulus parameterization scheme is good at the QPF of TC Rammasun. However, how does the KF scheme behave well? In the following, this question may be preliminarily answered by investigating the TC structures simulated by Expt. KF, which can be validated by NCEP/AVN analysis.

The TC warm core is indicated by the potential temperature anomalies at each pressure level in Fig. 7, which shows that, for the NCEP/AVN analysis (Fig. 7a), the warm core above 400 hPa is slantwise and inclined toward the north of the TC, which indicates that the potential large latent heat is released in the area north of the TC center. The maximum anomaly (3.6 K) is located vertically between 200 hPa and 300 hPa. The positive anomaly extends to a level between 800 hPa and 900 hPa, which covers a meridional swath of about 800 km. In Expt. KF (Fig. 7b), the overall structure of the warm core (especially the high-level inclination) is simulated successfully. Compared with NCEP/AVN analysis, the high-level inclination of the warm core is evident with the anomaly contour of 2 K extending toward the north and reaching the latitude of 29°N. The maximum anomaly (4.2 K) is located near 300 hPa. The positive anomaly extends to a lower level near 900 hPa with the similar swath of the NCEP/AVN analysis.

The comparison is also made for the upper-level divergence field between NCEP/AVN analysis (Fig. 8a) and Expt. KF (Fig. 8b). Figure 8a shows that the maximum divergence (6.4×10^{-5} s^{-1}) is located to the northeast (32.3°N, 127.5°E) of the TC center. This strong divergence makes possible the potential latent heat release in the north of the TC center and may account for the big anomaly of temperature and the inclination of the warm core indicated in Fig. 9. The distribution of divergence is well simulated in Expt. KF (Fig. 8b) with the maximum (6.9×10^{-5} s^{-1}) located at (32.1°N, 127.8°E), which is near to that of the NCEP/AVN analysis.

Figure 9 shows the vertical structures of wind and temperature by NCEP/AVN analysis (Fig. 9a) and Expt. KF (Fig. 9b). For the NCEP/AVN analysis, an evident asymmetric structure of horizontal wind speed is found around the TC center with the higher value in the north. The maximum wind speed in the north is 33 m s^{-1} and located near 850 hPa, while the one in the south is 21 m s^{-1} and located near 900 hPa. The 18 m s^{-1} contour almost reaches the pressure level of 300 hPa. This asymmetric structure is simulated in the KF experiment, in which the maximum is 36 m s^{-1} in the north and 24 m s^{-1} in the south.

Based on the above validations made on the MM5 model (with the Kain-Fristch cumulus parameterization scheme), the rainfall features and structure of TC Rammasun are reproduced and investigated in Section 7.

7. Preliminary analysis

To better understand the structure and rainfall fea-

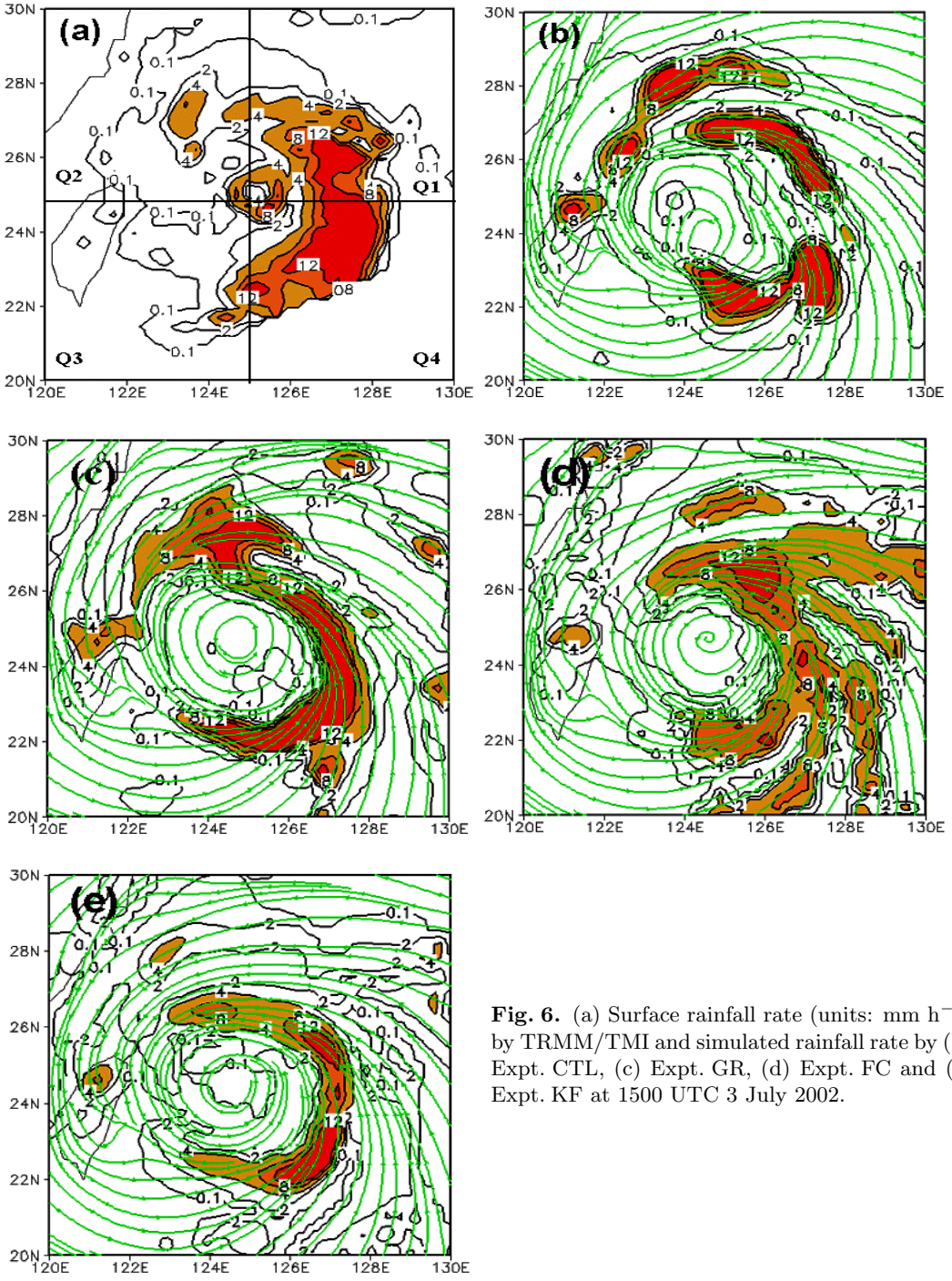

Fig. 6. (a) Surface rainfall rate (units: mm h^{-1}) by TRMM/TMI and simulated rainfall rate by (b) Expt. CTL, (c) Expt. GR, (d) Expt. FC and (e) Expt. KF at 1500 UTC 3 July 2002.

tures of TC Rammasun, three numerical simulations are carried out with the model that has been validated by Expt. KF (in section 6). Each of the three simulations concentrates on one of the three stages of TC Rammasun (see Table 3). Assumed as an average status for each of the three stages, during which the intensity and movement of the TC changes little, T1_avg (0000 UTC 29 June–0300 UTC 29 June), T2_avg (0000 UTC 3 July–0300 UTC 3 July) and T3_avg (1500 UTC 4 July–1800 UTC 3 July) are taken to represent T1, T2, and T3 respectively. The simulated surface rainfall rate, upper-level divergence, and low-level wind, averaged in the periods of T1_avg, T2_avg, and T3_avg respectively, are shown in Fig. 10. The vertical stru-

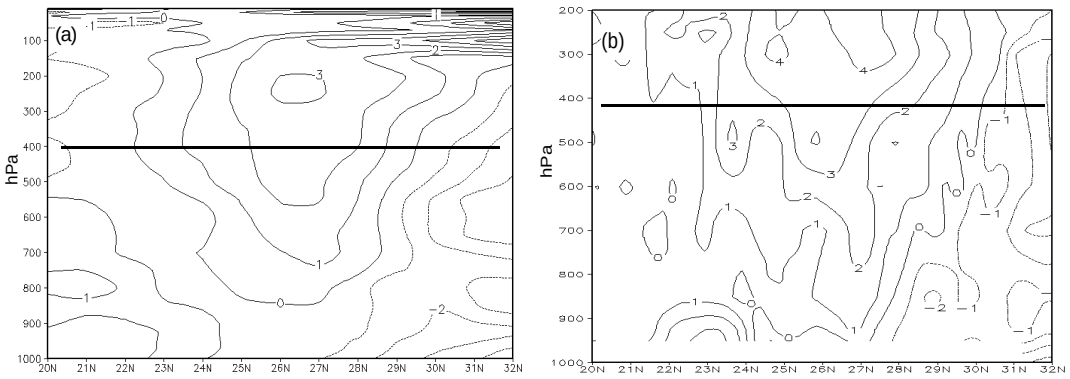

Fig. 7. The meridional vertical cross section along 124.4°E for potential temperature anomalies (units: K) by (a) NCEP/AVN analysis and (b) Expt. KF at 0000 UTC 4 July 2002.

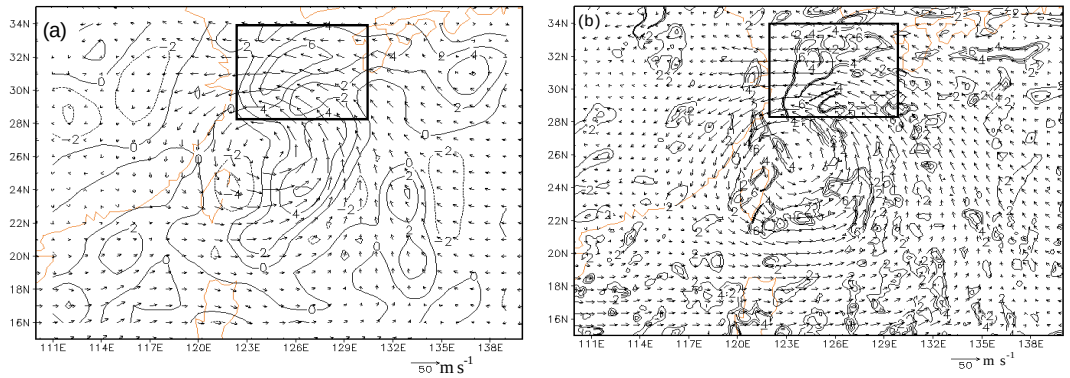

Fig. 8. The high-level divergence (averaged between 400 hPa and 100 hPa, units: $10^{-5}s^{-1}$) and low-level horizontal wind (averaged between 925 hPa and 700 hPa, units: m s^{-1}) by (a) NCEP/AVN analysis and (b) Expt. KF at 0000 UTC 4 July 2002. The rectangle denotes the studied area.

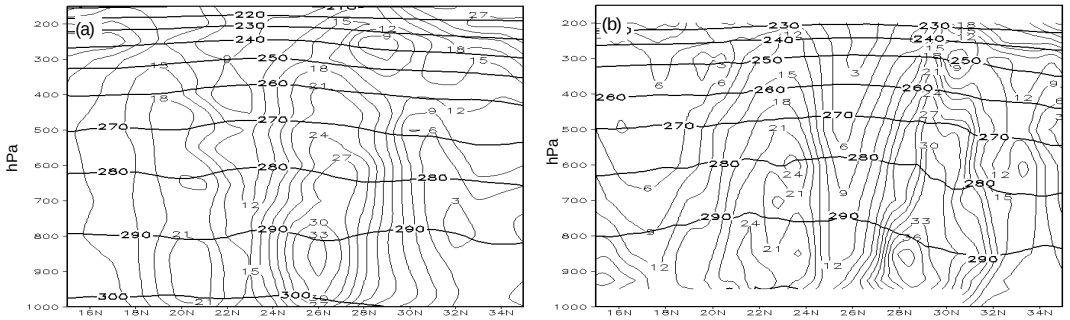

Fig. 9. The meridional vertical cross section of potential temperature (units: K) and horizontal wind speed (units: m s^{-1}) for (a) NCEP/AVN analysis and (b) Expt. KF at 0000 UTC 4 July 2002.

cture of simulated vertical wind speed and water content (cloud water and rain water are included) is shown in Fig. 11.

During the T1 period, the area of heavy rainfall rate (above 6 mm h^{-1}) is located south of the TC center with the high value in the southwest, where the upper-level divergence (maximum value of 4×10^{-5} s^{-1}) is stronger than elsewhere (Fig. 10a). High water content (10×10^{-4} kg kg^{-1}) in the area of heavy rainfall is mainly concentrated vertically under 500 hPa. The horizontal position of high water content corresponds well with the position of strong vertical motion. The maximum value (18×10^{-4} kg kg^{-1}) of water content is located between 700 hPa and 900 hPa, which is lower than the position (500 hPa–700 hPa) of the maximum vertical wind speed (1.2 m s^{-1}) (Fig. 11a).

When the TC develops into a typhoon, the distri-

Table 3. Three simulations for TC Rammasun.

Simulation	Simulation period	Description of TC status
T1	0000 UTC 28 June– 0000 UTC 1 July	Formation of tropical storm
T2	0000 UTC 2 July– 0000 UTC 4 July	Maintenance of typhoon
T3	0000 UTC 4 July– 0000 UTC 6 July	Decay period

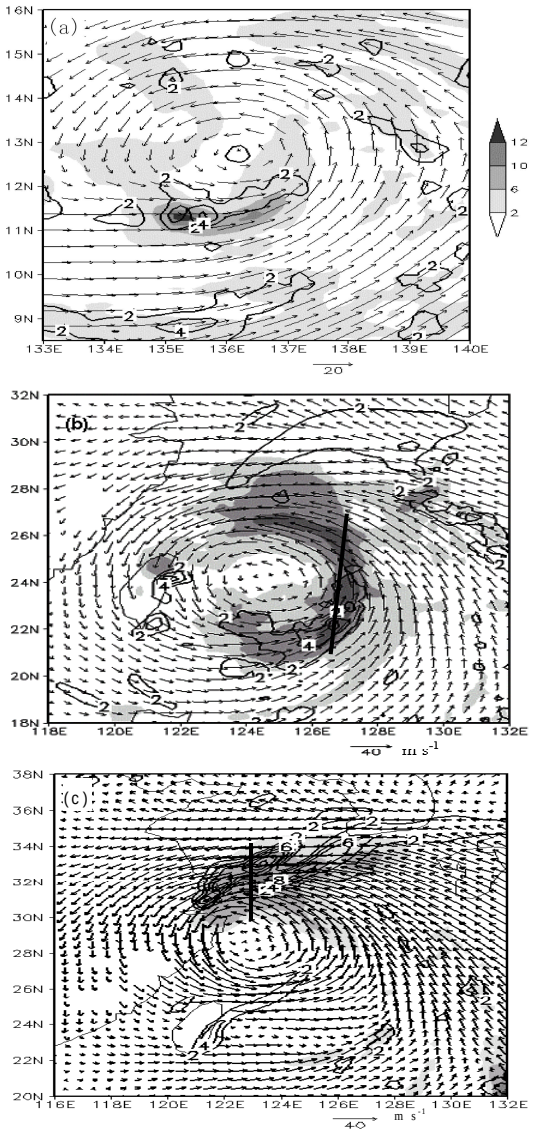

Fig. 10. Time-averaged surface rainfall rate (shaded, units: mm h^{-1}), low-level wind (averaged between 925 hPa and 700 hPa), high-level divergence (averaged between 400 Pa and 100 hPa, isolines, units:10^{-5} s^{-1}) by numerical simulations for the three periods of (a) T1_avg, (b) T2_avg, and (c) T3_avg. The thick line indicates the position of the cross section made in Fig. 11.

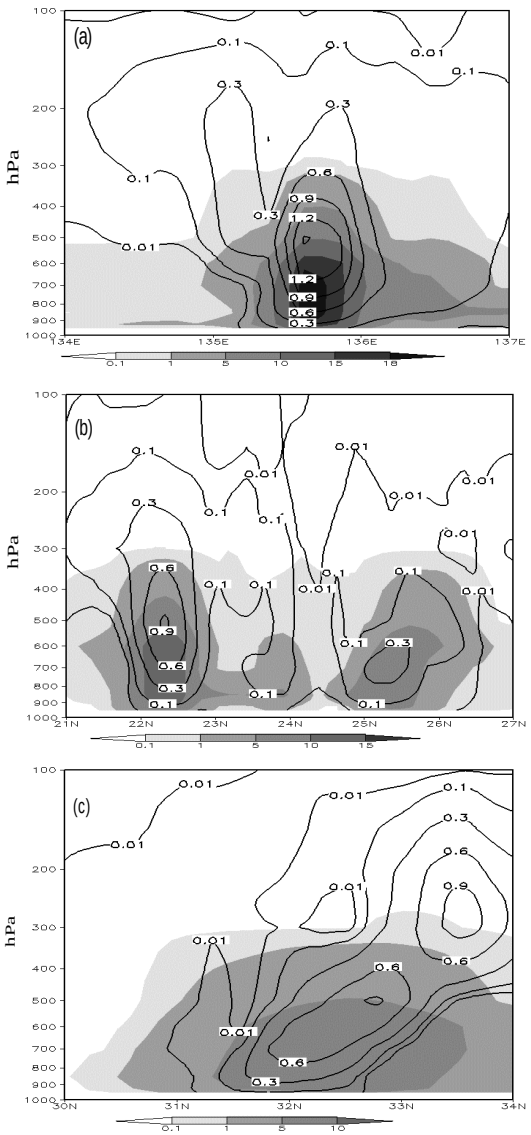

Fig. 11. The vertical cross sections of time-averaged vertical wind speed (isolines, units: m s^{-1}) and water content (shaded, units: 10^{-4} kg kg^{-1}) by numerical simulations along the thick line in Fig. 10 for the periods of (a) T1_avg, (b) T2_avg, and (c) T3_avg.

bution of rainfall rate is quite different from the former period. The rainfall is mainly concentrated around the east semi-circle of TC, with the maximum located in the southeast area, where the maximum divergence (4×10^{-5} s^{-1}) center exists (Fig. 10b). Asymmetry is evident in the distribution of high water content in the east semi-circle, the amount of which is higher in the south than in the north (Fig. 11b). The southern high water content (10×10^{-4} kg kg^{-1}) extends to a level of 600 hPa. The maximum value (13×10^{-4} kg kg^{-1}) of southern water content is located near 800 hPa, which is lower than the height (500–600 hPa) of the maximum vertical wind speed (0.9 m s^{-1}). The position of the maximum value (8×10^{-4} kg kg^{-1}) of northern water content is also located near 800 hPa, above which (700 hPa) the maximum vertical wind speed (0.3 m s^{-1}) exists.

During the T3 period, the rainfall area moves to the north quadrant of the TC, which is also the region of major divergence (8×10^{-5} s^{-1}). The distance between the location of the maximum rainfall (12 mm h^{-1}) and the TC center position is about 400 km (Fig. 10c). The rainfall intensity is no less than that in the T2 period. The water content (5×10^{-4} kg kg^{-1}) and vertical velocity (0.3 m s^{-1}) are still very large especially in the area of the intensive rainfall (Fig. 11c). The 5×10^{-4} kg kg^{-1} contour of water content reaches the height of 600 hPa, and the position (800 hPa) of the maximum value (7×10^{-4} kg kg^{-1}) is lower than the location (above 600 hPa) of the maximum vertical wind speed (0.9 m s^{-1}). The slantwise distribution feature of vertical wind speed is quite different than that of T1 and T2, which may indicate the decay of the TC.

8. Summary and discussions

TRMM data (TMI/PR/VIRS) and a numerical model are used to investigate the structure and rainfall features of TC Rammasun (2002).

Based on the analysis of the available TRMM data at several instances, the typical features for the 3-D structure of the TC rainfall (PW) is preliminarily understood.

Assumed to be an indicator of the energy that the TC can obtain by the convective motion, SCAPE is diagnosed with NCEP/AVN analysis and connected with the surface rainfall rate by TRMM/TMI. It is found that the high positive SCAPE is located just inside the area of high rainfall rate.

Considering the limitation of TRMM data, according to its time resolution and coverage, the data cannot cover the whole process of the TC. To better understand the structure and rainfall features of TC Rammasun, numerical experiments are carried out based on the validation of the MM5 model. It is found from the simulations that the intensity of rainfall cannot be simply determined by the period that the TC is undergoing. The position of maximum rainfall is located in the area of strong vertical motion and the upper-level intensive divergence. The height to which the maximum vertical motion extends corresponds with the amount of rainfall. The water content of TC Rammasun is mainly concentrated under 600 hPa, the center of which is located near 800 hPa, which is lower than the position (above 700 hPa) of maximum vertical wind speed.

This study has demonstrated some characteristics of TC Rammasun's structure and rainfall, but it is still preliminary. It is recognized that a preferred way to improve the simulation of the structure and rainfall of the TC would be to assimilate the TRMM data directly into the mesoscale model with high resolution, which is in progress and will be reported in a future study.

Acknowledgments. This work was supported by the National Natural Science Foundation of China (Grant Nos. 49975014, 40275018 and 40333025) and National Social Development Research Programme granted by The Ministry of Science and Technology.

REFERENCES

Dudhia, J., 1993: A nonhydrostatic version of the Penn State-NCAR mesoscale model: Validation tests and simulation of an Atlantic cyclone and cold front. *Mon. Wea. Rev.*, **121**, 1493–1513.

Emanuel, K. A., 1983a: The Lagrangian parcel dynamics of moist symmetric instability. *J. Atmos. Sci.*, **40**, 2368–2375.

Emanuel, K. A., 1983b: On assessing local conditional symmetric instability from atmospheric soundings. *Mon. Wea. Rev.*, **111**, 2016–2033.

Fritsch, J. M., and C. F. Chappell, 1980: Numerical prediction of convectively driven mesoscale pressure systems. Part I: Convective parameterization. *J. Atmos. Sci.,* **37**, 1722–1733.

Grell, G., 1993: Prognostic evaluation of assumptions used by cumulus parameterizations. *Mon. Wea. Rev.*, **121**, 764–787.

Grell, G. A., J. Dudhia, and D. R. Stauffer, 1994: A description of the fifth generation Penn State/ NCAR mesoscale model (MM5). NCAR Tech. Note NCAR/TN-398+STR, 138pp.

Jin Xin, Li Wanbiao, and Zhu Yuanjing, 2003: A study on the Meiyu Front using TRMM/PR data during the 1998 GAME/HUBEX. *Adv. Atmos. Sci.*, **20**, 293–298.

Kain, J. S., and J. M. Frisch, 1993: Convective parameterization for mesoscale models: The Kain-Fritsch scheme. *The Representation of Cumulus Convection in Numerical Models*, *Meteor. Monogr.*, Amer. Meteor. Soc., **46**, 165–170.

Kummerow, C., W. Barnes, T. Kozu, J. Shiue, and J. Simpson, 1998: The Tropical Rainfall Measuring Mission (TRMM) Sensor Package. *J. Atmos. Oceanic Technol.*, **15**, 809–817.

Kuo, Y., R. J. Reed, and Y. Liu, 1996: The ERICA IOP 5 storm. Part III: Mesoscale cyclogenesis and precipitation parameterization. *Mon. Wea. Rev.,* **124**, 1409–1434.

Marécal, V., and J. F. Mahfouf, 2001: Four-dimensional variational assimilation of total column water vapor in rainy areas. *Mon. Wea. Rev.*, **130**, 43–58.

Pu, Z.-X., W.-K. Tao, S. Braun, J. Simpson, Y. Jia, J. Halverson, A. Hou, and W. Olson, 2002: The impact of TRMM Data on mesoscale numerical simulation of supertyphoon Paka. *Mon. Wea. Rev.*, **130**, 2448–2458.

Rodgers, E., W. Olson, J. Halverson, J. Simpson, and H. Pierce, 2000: Environment forcing of Supertyphoon Paka's (1997) latent heat structure. *J. Appl. Meteor.*, **39**, 1983–2006.

Shutts, G. J., 1990: SCAPE charts from numerical weather prediction model fields. *Mon. Wea. Rev.*, **118**, 2745–2751.

Simpson, J., C. Kummerow, W.-K. Tao, and R. F. Adler, 1996: On the Tropical Rainfall Measuring Mission (TRMM). *Meteor. Atmos. Phys.*, **60**, 19–36.

Weygandt, S., and N. L. Seaman, 1994: Quantification of predictive skill for mesoscale and synoptic-scale meteorological features as a function of horizontal grid resolution. *Mon. Wea. Rev.*, **122**, 57–71.

Wang, W., and N. L. Seaman, 1997: A comparison study of convective parameterization schemes in a mesoscale model. *Mon. Wea. Rev.*, **125**, 252–278.

Xu Zhifang, Ge Wenzhong, Dang Renqing, Toshio Iguchi and Takao Takada, 2003: Application of TRMM/PR data for numerical simulation with mesoscale model MM5. *Adv. Atmos. Sci.*, **20**, 185–193.